Dielectronic satellite spectra of hydrogenlike titanium (Ti XXII)

M. Bitter, S. von Goeler, S. Cohen, K. W. Hill, S. Sesnic, F. Tenney, and J. Timberlake
Plasma Physics Laboratory, Princeton University, Princeton, New Jersey 08544

U. I. Safronova
Institute for Spectroscopy, Troitsk, Podolsky District 142092, Union of Soviet Socialist Republics

L. A. Vainshtein
Lebedev Physical Institute, Moscow 117924, Union of Soviet Socialist Republics

J. Dubau and M. Loulergue
Observatoire de Paris, F-92190 Meudon, France

F. Bely-Dubau and L. Steenman-Clark
Observatoire de Nice, Boîte Postale No. 252, F-06007 Nice Cedex, France
(Received 2 June 1983)

High-resolution spectra of the Ly-α_1 and Ly-α_2 lines of hydrogenlike titanium, Ti XXII, and the associated dielectronic satellites which are due to transitions $1snl$-$2pnl$ with $n \geq 2$, have been observed from tokamak discharges with auxiliary ion-cyclotron heating with central electron temperatures of 2 keV and central electron densities of 8×10^{13} cm^{-3} on the Princeton Large Torus (PLT). The data have been used for a detailed comparison with theoretical predictions based on the Z-expansion method and on the multiconfiguration Thomas-Fermi—potential wave-function method (SUPERSTRUCTURE code). The predictions from the Z-expansion method are in excellent agreement with the observed spectral data except for minor discrepancies between the theoretical and experimental wavelengths of 0.0003 Å for the $n=2$ satellites and of 0.0001 Å for the separation of the Ly-α_1 and Ly-α_2 lines. The latter discrepancy is, however, removed if the Lamb shift and relativistic effects of order α^4 are taken into account. Very good agreement with the experimental wavelengths is also obtained for the results from SUPERSTRUCTURE though somewhat larger and systematic discrepancies ($\simeq$0.0009 Å) exist. The observed spectra have been used for diagnosis of the central ion and electron temperatures of the PLT discharges and for a measurement of the total dielectronic recombination rate coefficient of Ti XXII. The measured rate coefficient is in good agreement with the predictions from both the detailed calculations and Burgess's general formula.

I. INTRODUCTION

Spectra of hydrogenlike titanium Ti XXII are presented in this paper. The spectra have been observed from tokamak discharges with central electron temperatures in excess of 2 keV on the Princeton Large Torus (PLT) using a high-resolution crystal spectrometer. The high electron temperatures produced by ion-cyclotron resonance heating (ICRH) and the good spectral resolution have made it possible to obtain for the first time detailed experimental data on the dielectronic satellites of the Ly-α_1 and Ly-α_2 lines of Ti XXII and to perform a detailed comparison with theoretical calculations. The spectra have also been used for measurements of the central ion and electron temperature in the hot core of PLT discharges and for a determination of the total dielectronic recombination rate coefficient of Ti XXII.

The spectra of hydrogenlike ions are of fundamental importance for the study of multiply charged heavy ions. This is true, in particular, with regard to relativistic effects which are most evident from the fine-structure splitting of the $1s$-$2p$ resonance line. The resonance-line splitting strongly increases with atomic number Z. Whereas the separation of the fine-structure components of the resonance lines of low-Z hydrogenlike ions is very small and usually masked by Doppler broadening, the doublet is well-resolved for ions such as Ti XXII. For exact wavelength calculations it is necessary to also include QED effects due to self-energy and vacuum polarization such as the Lamb shift.[1]

In addition to the resonance lines, the spectra of high-Z hydrogenlike ions show a series of dielectronic satellites which are due to transitions of the type $1snl$-$2pnl$ with $n \geq 2$. The $2pnl$ states are doubly excited heliumlike states above the ionization limit of the heliumlike ion. These states can autoionize to the hydrogenlike ground state, or they can decay by a stabilizing radiative transition to a singly excited heliumlike state. The latter transition gives rise to a satellite line. Since the radiative decay probability increases with Z^4 along the isoelectronic sequence, whereas the autoionization probability is approximately independent of Z, the satellite lines are relatively intense compared with the resonance line only for ions with $Z \geq 20$. In low-density plasmas the $2pnl$ states are not

populated from the heliumlike $1s^2$ ground state by electron impact excitation since double collisions are highly improbable. The satellites can, therefore, only be produced by the dielectronic recombination of hydrogenlike ions. This is different from the previously well-documented satellite spectra of heliumlike ions[2–7] where dielectronic recombination and collisional inner-shell excitation are both important. The satellite spectra of hydrogenlike ions observed from low-density plasmas are, therefore, of great interest for a study of the dielectronic recombination process. Spectra of the Ly-α_1 and the Ly-α_2 lines and their associated satellites are currently also studied in beam-foil experiments[8,9] and in laser-produced plasmas.[10] The excitation mechanisms for the satellite lines are, however, less well-defined in these experiments than for low-density plasmas.[11]

Tokamak plasmas are currently the best suited low-density laboratory plasma for observation of the line spectra from highly ionized ions. In fact, it is now possible to obtain large volume tokamak plasmas with central electron densities of $0.1-1\times10^{15}$ cm^{-3} and electron temperatures in the range from 1 to 3 keV under quasi-steady-state conditions for periods of 100–300 ms. Under these conditions the relative abundance and spatial distribution of the different states of ionization of high-Z elements approximate coronal equilibrium. Since tokamak plasmas are also the best diagnosed high temperature plasmas, they are very appropriate for experimental testing of atomic theories of the spectra of multiply charged ions. On the other hand, the spectra of high-Z ions will be of increasing importance for diagnosis of central plasma parameters in the next generation of large tokamaks, for which central electron and ion temperatures in excess of 10 keV are predicted. In particular, determination of the central ion temperature from Dopler broadening of the resonance lines of hydrogenlike ions with $Z \geq 20$ will be of vital importance for future tokamak experiments.

II. EXPERIMENTAL SETUP

Hydrogenlike titanium, Ti XXII, can be produced in hot plasmas under coronal-equilibrium conditions[12] with a fractional abundance of 10% if the electron temperature exceeds 2 keV (see Fig. 1). Plasmas of sufficiently high electron temperatures are presently obtained in the core of large tokamaks with use of additional heating schemes. Nevertheless, it is experimentally difficult to produce these ions in appreciable amounts since significant deviations from the ideal charge-state distribution can occur in tokamak plasmas as a result of the radial particle transport.[13] Coronal equilibrium is approached only if the characteristic confinement time of an ion is long compared with the ionization and recombination times.[14,15] This condition is especially hard to fulfill for hydrogenlike ions because the ionization and recombination times are considerably longer for these ions than for ions of the lower charge states. This is due to the high ionization potential of the heliumlike ions ($E_I = 6.249$ keV for Ti XXI) and due to the fact that dielectronic recombination—the dominant mechanism of recombination for ions below the heliumlike charge state—is comparatively unimportant. Since the confinement time increases with plasma density, whereas the recombination and ionization times are inversely proportional to the electron density, the most efficient way to enhance the concentration of hydrogenlike ions is to perform the experiments at high plasma densities.

In PLT discharges with additional ion-cyclotron heating (ICRF) of 4 MW at 25 MHz it has been possible to produce plasmas with central electron densities of $\simeq 1\times10^{14}$ cm^{-3} and central electron temperatures of 2 to 3 keV with a minor radius of 40 cm in quasi-steady-state for periods of 200 to 300 ms. Even under these conditions the characteristic time for radial transport of hydrogenlike titanium ions as determined from titanium injection ex-

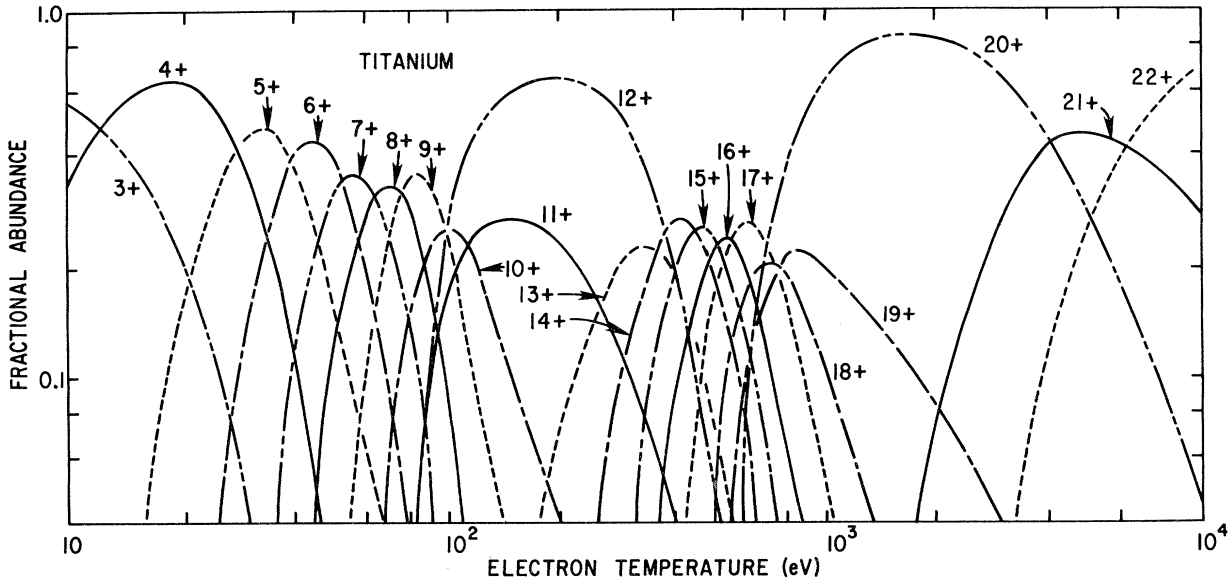

FIG. 1. Fractional abundance of the different states of ionization of titanium for coronal-equilibrium conditions (Ref. 12).

periments was only about one-third the ionization time ($\simeq$100 ms) of the heliumlike Ti XXI ions.[16] Transport was, therefore, important in our experiments. We may assume that the radial density profile of the Ti XXII ions was wider and the relative abundance of the Ti XXII and Ti XXI charge states in the center of the plasma was smaller than the coronal-equilibrium values, shown in Fig. 1, although we did not measure these radial ion charge-state distributions. A further experimental difficulty arises from the fact that the dielectronic satellite lines are relatively intense only at low electron temperatures. The spectra of greatest interest are, therefore, emitted at temperatures for which the hydrogenlike ions are not the most abundant charge state. Under these conditions the background radiation from the bremsstrahlung and the radiative recombination continuum can be comparable to or even larger than the observed line radiation and it is, therefore, difficult to obtain spectra with a small statistical error.

Titanium is used in the PLT tokamak as a material for the Faraday shields of the rf antennas and as a getter for low-Z impurities. During the ohmic heating phase with electron temperatures of 1 to 1.5 keV the line radiation from hydrogenlike titanium Ti XXII is smaller than the background radiation. With rf heating it is, however, enhanced due to both an increase in the amount of titanium in the discharge and an increase in the central electron temperature. Most of the data have, therefore, been taken under these conditions. In a series of discharges the titanium concentration has been increased by injection of titanium using the laser blowoff technique.[17] In these experiments a controlled amount of titanium was induced by directing a laser beam of adjustable cross section and power against a titanium target. This technique also made it possible to identify unambiguously the observed radiation as titanium lines.

The data were recorded by a high-resolution ($\lambda/\Delta\lambda=15\,000$, at $\lambda=2.5$ Å) curved crystal spectrometer which permitted simultaneous observation of spectrum lines in the wavelength range from 2.485 to 2.525 Å. The spectrometer consisted of a ($20\bar{2}\bar{3}$; $2d=2.7497$ Å) quartz crystal and a position-sensitive multiwire proportional counter[18] in the Johann configuration.[19] The dimensions of the crystal and its radius of curvature were $6\times1.5\times0.030$ in. and 367.8 cm, respectively. The spectrometer is very similar to the one previously used for observation of the dielectronic satellite spectrum of heliumlike titanium Ti XXI[7] and Doppler broadening measurements on the PDX (poloidal divertor experiment) tokamak.[20] Instrumental details have been described by Bitter *et al.*[21]

Figure 2 shows spectra accumulated from 17 PLT discharges during consecutive time intervals from 600 to 650 and 650 to 700 ms. Ion-cyclotron heating of 4 MW was applied during the period from 500 to 700 ms, and titanium was injected at the time of 650 ms. The line radiation is consequently enhanced by about a factor of 2 in the spectrum of Fig. 2(b), which was obtained immediately after the titanium injection. Typical profiles of the laser Thomson scattering data for these PLT discharges exhibiting a central electron temperature of 2 keV and a central electron density of 8×10^{13} cm^{-3} are shown in Fig. 3. In

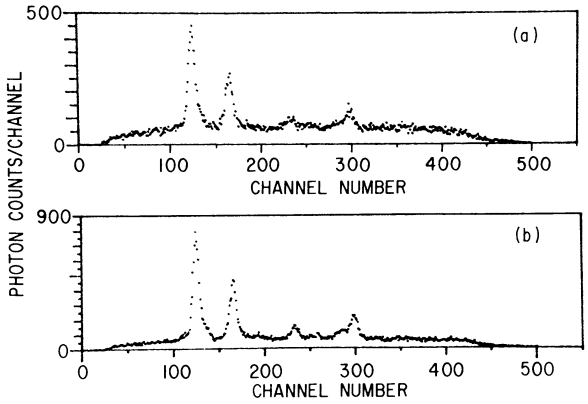

FIG. 2. Satellite spectra of Ti XXII. The data have been accumulated from 17 PLT discharges with additional ion-cyclotron heating of 4 MW during consecutive time intervals from (a) 600 to 650 ms and (b) 650 to 700 ms. An approximate amount of 1.5×10^{17} titanium atoms was injected into each discharge at the time of 650 ms.

addition to the Ti XXII line radiation, the spectra in Fig. 2 show a relatively intense background from the radiation continuum. An approximate number of 1.5×10^{17} titanium atoms was injected into each discharge. Some data were taken with an improved time resolution of 15 ms to study the time history of the Ti XXII spectrum lines. From these measurements we obtained values in the range from 20 to 30 ms for the confinement time of the Ti XXII ions. The titanium injection experiments also made it possible to obtain an estimate of the total number of titanium atoms that are normally present in the discharge from the Faraday shields and the titanium gettering. By comparing the intensities of the titanium line radiation observed before and immediately after injection, we conclude that the titanium supply from these sources was comparable to the injected titanium.

In order to reduce the statistical error and to distinguish clearly the Ti XXII and Ti XXI spectral features from the background radiation, the spectrum shown in Fig. 4 was accumulated from 78 rf heated PLT discharges with almost identical parameters. The dashed line between B and D indicates the background level of the radiation continuum. The background is constant except for a slight reduction observed at the lower channel numbers. This intensity reduction, which is less than 5% in the immediate vicinity of spectral feature 1, is caused by a vignetting effect of the beryllium window on the PLT tokamak. For a detailed comparison with theoretical predictions the data points at the channel numbers from 87 to 145 have been corrected for this geometrical effect. The intensity correction factors were determined from a linear interpolation of the background radiation represented by the dashed line between A and C.

III. EXPERIMENTAL RESULTS AND THEORETICAL PREDICTIONS

Spectra of hydrogenlike ions have been previously observed from solar flares and from tokamak plasmas for

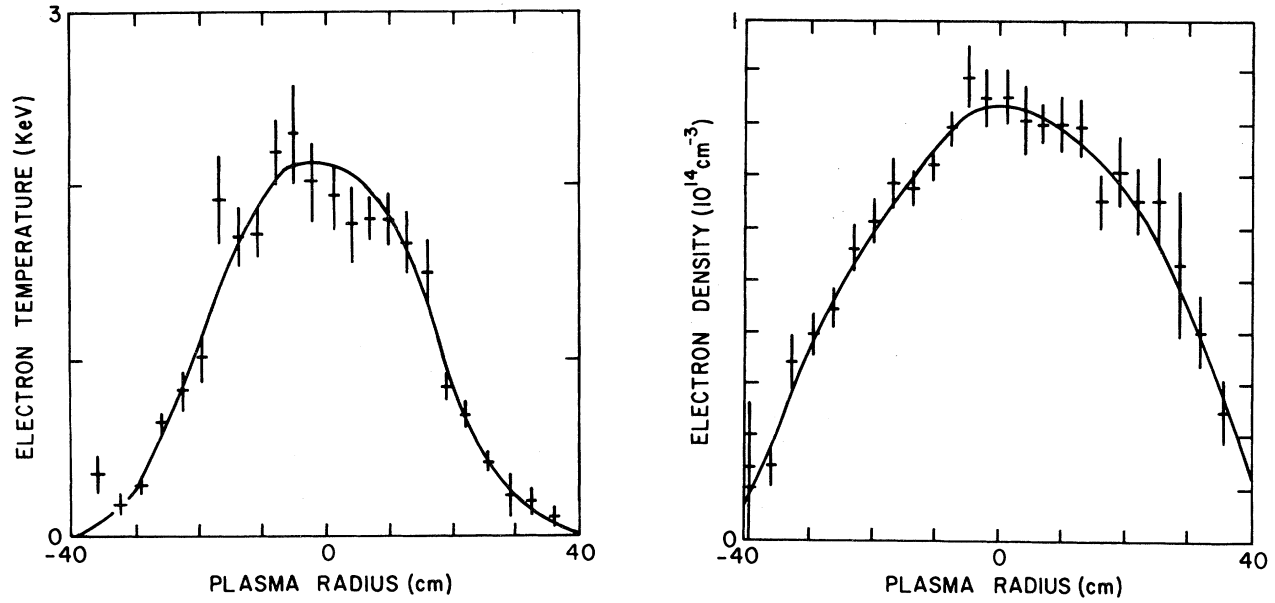

FIG. 3. Typical electron-density and electron-temperature profiles of PLT discharges with 4 MW ion-cyclotron heating as obtained from laser Thomson scattering.

$Z \leq 26$.[22–26] These observations have well-confirmed the predicted Z dependence both for the doublet splitting of the resonance line and the intensity of the dielectronic satellites. The Z dependence of these spectral features is illustrated in Figs. 5(a) and 5(b) which present spectra of hydrogenlike ions for $Z=8$, 12, 16, 20, and 26. For O VIII and Mg XII the separation of the Ly-α doublet is smaller than the Doppler width, whereas for S XVI, Ca XX, and Fe XXVI the fine-structure components of the resonance line are clearly resolved. Similarly, the $1snl$-$2pnl$ dielectronic satellites are not observed in the spectra of O VIII and Mg XII, but they appear in the spectrum of S XVI, and are clearly noticeable in the solar-flare spectra of Ca XX and Fe XXVI. However, the statistical error of these data has not permitted a detailed comparison with theoretical predictions. An interesting result is the observation of intensity ratios in the range from 0.5 to 0.8 for the Ly-α_2 and the Ly-α_1 lines of S XVI on the Alcator experiment.[23] This departure from the value of 0.5 has been ascribed to excitation of the $2P_{3/2}$ and $2P_{1/2}$ states from the metastable $2S_{1/2}$ state by proton collisions.[27]

In this section we give a detailed comparison of the observed Ti XXII spectra with new theoretical calculations. Two methods are used to calculate atomic parameters (wavelengths, and autoionization and radiative transition probabilities) for dielectronic satellites: the Z-expansion method[28] and the multiconfiguration Thomas-Fermi—potential wave-functions method which utilizes the program SUPERSTRUCTURE.[29,30] A comparison of the results obtained by different methods of calculation with experimental data is of great interest for the atomic theory of multiply charged high-Z ions as well as for the diagnosis of astrophysical and laboratory plasmas. Table I lists the experimental wavelengths and theoretical results for the most prominent spectral features which have been identified as the $1s(^2S_{1/2})$-$2p(^2P_{3/2})$ and the $1s(^2S_{1/2})$-$2p(^2P_{1/2})$ fine-structure components of the resonance transition, or the Ly-α_1 and the Ly-α_2 lines (features 1 and 2), and the well-resolved $1snl$-$2pnl$ dielectronic satellites with $n=2$ (features 3—8). The experimental wavelengths have been determined relative to the Ly-α_2 line for which we adopted the value of 2.4957 Å.[31] This value was obtained in the approximation of the present calculations, which do not include radiative corrections and relativistic corrections of the fourth or higher orders in the fine-structure constant α ($\alpha=1/137.036$). The radiative and higher-order relativistic corrections provide a general increase of all the wavelengths and relative shifts of individual lines by approximately 0.09 mÅ. In particular, for the Ly-α_1 and Ly-α_2 lines of Ti XXII we obtain the values of 2.4912 and 2.4966 Å,[32] which are in agreement with the results of Erickson.[1] The separation of the fine-structure components in the present experiment is 0.0054 Å in accordance with these very detailed theoretical predictions.

The structures observed on the wings of the Ly-α_1 and the Ly-α_2 lines are ascribed to $1snl$-$2pnl$ dielectronic satellites with $n \geq 3$. Contrary to the $n=2$ satellites, the $n \geq 3$

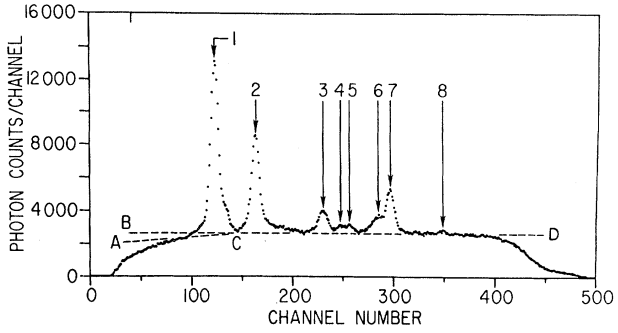

FIG. 4. Satellite spectrum of Ti XXII accumulated from 78 rf heated PLT discharges with typical parameters shown in Fig. 3.

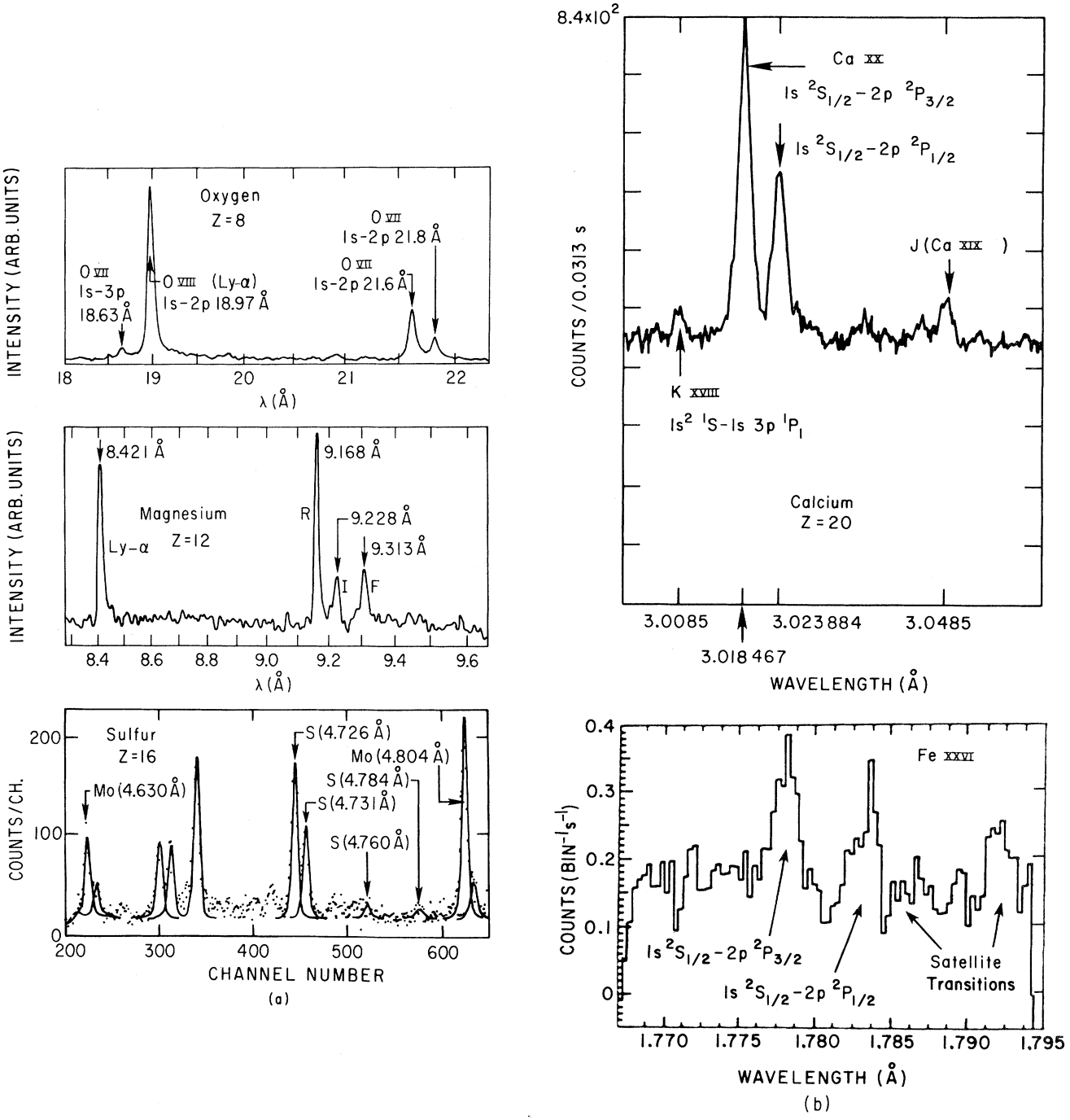

FIG. 5. (a) Spectra of hydrogenlike oxygen O VIII, magnesium Mg XII, and sulfur S XVI. The spectra have been observed from the PLT and Alcator tokamaks. (b) Spectra of hydrogenlike calcium Ca XX and iron Fe XXVI from solar flares. The spectra in (a) and (b) illustrate the Z dependence of the doublet splitting of the Ly-α lines and the intensities of the dielectronic satellites.

satellites can be uniquely assigned to one of the fine-structure components as the parent line. This is due to the fact that the electrostatic interaction between the $2p$ electron and the nl spectator electron, which is responsible for the satellite-to-resonance-line separation, scales as n^{-3} and is smaller than the $2p$ spin-orbit interaction if $n \geq 3$. The Ly-α_1 and the Ly-α_2 lines thus represent the series limits for these satellites which are approached with an increasing main quantum number n for the spectator electron. The number of satellite transitions increases with n as n^2. However, since the autoionization probability A_a decreases with n as n^{-3} (and also decreases rapidly with increasing l for $l \geq 3$),[33,34] the satellite intensity also decreases with increasing n. Detailed calculations of the

TABLE I. Experimental wavelengths and theoretical predictions from the Z-expansion method (superscript 1) and from SUPERSTRUCTURE (superscript 2) for the Ly-α lines of Ti XXII and the $n=2$ satellites. Wavelengths are in Å. Radiative probability A_r, autoionization probability A_a, and line factors $F_2(s)$ are in 10^{13} s^{-1}. Key letters agree with Safronova's notation.

Peak	Key	Array	λ_{expt}	λ_{theor}	A_a	A_r	$\sum A_r$	$F_2(s)$
1		$1s(^2S_{1/2})$-$2p(^2P_{3/2})$	2.4903	2.4904[1]		15.00[1]		
				2.4903[2]		14.45[2]		
	V	$1s\,2s(^3S_1)$-$2s\,2p(^1P_1)$		2.4915[1]	20.00[1]	0.25[1]	14.70[1]	0.42[1]
				2.4905[2]	16.94[2]	0.19[2]	13.60[2]	0.31[2]
2		$1s(^2S_{1/2})$-$2p(^2P_{1/2})$	2.4957[a]	2.4957[1]		14.90[1]		
				2.4956[2]		14.36[2]		
	M	$1s\,2p(^1P_1)$-$2p^2(^1S_0)$		2.4973[1]	3.00[1]	24.30[1]	24.30[1]	2.67[1]
				2.4960[2]	2.70[2]	22.96[2]	22.99[2]	2.42[2]
3	*T*	$1s\,2s(^1S_0)$-$2s\,2p(^1P_1)$	2.5044	2.5046[1]	20.00[1]	14.50[1]	14.60[1]	25.00[1]
				2.5027[2]	16.94[2]	13.40[2]	13.6[2]	22.29[2]
	K	$1s\,2p(^3P_2)$-$2p^2(^1D_2)$		2.5052[1]	30.60[1]	3.93[1]	29.04[1]	10.10[1]
				2.5042[2]	27.69[2]	3.11[2]	26.94[2]	7.88[2]
4	*Q*	$1s\,2s(^3S_1)$-$2s\,2p(^3P_2)$	2.5066	2.5070[1]	1.36[1]	14.50[1]	14.5[1]	6.21[1]
				2.5066[2]	1.29[2]	13.67[2]	13.67[2]	5.88[2]
5	*B*	$1s\,2p(^3P_1)$-$2p^2(^3P_2)$	2.5077	2.5081[1]	6.72[1]	8.19[1]	28.89[1]	7.72[1]
				2.5070[2]	5.01[2]	7.57[2]	27.20[2]	5.89[2]
	R	$1s\,2s(^3S_1)$-$2s\,2p(^3P_1)$		2.5108[1]	1.67[1]	14.20[1]	14.45[1]	4.43[1]
				2.5101[2]	1.52[2]	13.48[2]	13.67[2]	4.05[2]
6	*A*	$1s\,2p(^3P_2)$-$2p^2(^3P_2)$	2.5115	2.5116[1]	6.72[1]	17.80[1]	28.95[1]	16.80[1]
				2.5106[2]	5.01[2]	17.33[2]	27.20[2]	13.48[2]
	S	$1s\,2s(^3S_1)$-$2s\,2p(^3P_0)$		2.5122[1]	1.36[1]	14.40[1]	14.39[1]	1.24[1]
				2.5115[2]	1.30[2]	13.67[2]	13.67[2]	1.19[2]
	F	$1s\,2p(^3P_1)$-$2p^2(^3P_0)$		2.5126[1]	0.25[1]	27.40[1]	27.74[1]	0.24[1]
				2.5113[2]	0.17[2]	26.12[2]	26.41[2]	0.16[2]
7	*J*	$1s\,2p(^1P_1)$-$2p^2(^1D_2)$	2.5130	2.5132[1]	30.60[1]	25.10[1]	29.16[1]	64.40[1]
				2.5123[2]	27.69[2]	23.82[2]	26.94[2]	60.36[2]
8	*G*	$1s\,2p(^1P_1)$-$2p^2(^3P_2)$	2.5195	2.5196[1]	6.72[1]	2.97[1]	28.93[1]	2.80[1]
				2.5187[2]	5.01[2]	2.29[2]	27.20[2]	1.78[2]
	P	$1s\,2p(^3P_1)$-$2s^2(^1S_0)$		2.5272[1]	32.90[1]	1.37[1]	5.36[1]	1.18[1]
				2.5266[2]	29.39[2]	1.12[2]	5.24[2]	0.95[2]
	O	$1s\,2p(^1P_1)$-$2s^2(^1S_0)$		2.5388[1]	32.90[1]	4.13[1]	5.70[1]	3.54[1]
				2.5385[2]	29.39[2]	4.11[2]	5.24[2]	3.49[2]

[a]The experimental wavelengths are normalized to the theoretical value of 2.4957 Å for the $1s(^2S_{1/2})$-$2p(^2P_{1/2})$ transition.

atomic parameters for all the $1snl$-$2pnl$ transitions, which can be associated with the spectator electron in a certain n-shell, have been performed for n values up to five. The $n \geq 6$ satellites are then obtained by a line-by-line extrapolation from a selected set of $n=5$ satellites with use of the appropriate scaling laws.[34] Tables II—IV list the theoretical predictions of the Z-expansion method and the SUPERSTRUCTURE calculations for the satellites with $n=3-5$. Included in the tables are only the most intense transitions with line factors $F_2(s) \geq 5\times 10^{11}$ s^{-1}. It should be noted that the two sets of theoretical values for λ, A_r, A_a, and $F_2(s)$ are in close agreement: For the wavelengths the relative differences are smaller than 10^{-3} and for the line factors $F_2(s)$ of the most important lines, they are $\simeq 10^{-1}$. Nevertheless, since we analyze spectra of very high resolution ($\lambda/\Delta\lambda=15\,000$) the discrepancies of the wavelengths are apparent. The values calculated with SUPERSTRUCTURE are smaller by 1 to 2 mÅ than those obtained by the Z-expansion method. In order to reduce this difference a shift of 0.0009 Å can be applied to all the two-electron-system wavelengths calculated with SUPERSTRUCTURE. A comparison of the two theoretical predictions for the line factors $F_2(s)$ with the experimental data is more difficult unless the uncertainties due to the experimental errors for the relative line intensities and the electron temperature are less than 10%. Since the satellites with $n \geq 3$ fall into a very narrow wavelength range and are partially blended with the resonance line, a detailed comparison between experiment and theory can only be made by use of synthetic spectra.

Figures 6 and 7 present the experimental data and the synthetic spectra (solid lines), which have been obtained by calculating Voigt profiles for the transition arrays given in Tables I—IV. In addition to the fine-structure components $1s(^2S_{1/2})$-$2p(^2P_{3/2})$ and $1s(^2S_{1/2})$-$2p(^2P_{1/2})$ of the Ti XXII resonance line, the theoretical spectra include the contribution from 14 $n=2$ satellites (curve II), 58 $n=3$ satellites (curve III), 58 $n=4$ satellites (curve IV), and 46 $n=5$ satellites (curve V). Curve I represents the total intensity of all these spectrum lines. An intensity ra-

TABLE II. Atomic data for satellites of the Ti XXII resonance line due to transitions $1s\,3l$-$2l'3l''$ from the Z-expansion method (superscript 1) and from SUPERSTRUCTURE (superscript 2). Wavelengths are in Å. Radiative probability A_r, autoionization probability A_a, and line factors $F_2(s)$ are in 10^{13} s^{-1}.

Array	λ^1	λ^2	A_a^1	A_a^2	A_r^1	A_r^2	$\sum A_r^1$	$\sum A_r^2$	$F_2^1(s)$	$F_2^2(s)$
$1s\,3p(^1P_1)$-$2p\,3p(^1S_0)$	2.4874	2.4852	1.60	1.37	12.80	11.32	16.10	14.50	1.16	0.97
$1s\,3p(^1D_2)$-$2p\,3d(^1P_1)$	2.4878	2.4858	0.10	0.08	13.30	11.30	14.54	14.11	0.25	0.19
$1s\,3d(^3D_2)$-$2p\,3d(^1F_3)$	2.4881	2.4863	2.40	1.80	4.92	4.18	15.10	15.70	4.72	3.00
$1s\,3s(^3S_1)$-$2p\,3s(^1P_1)$	2.4883	2.4864	8.58	6.17	0.71	0.49	11.40	10.60	0.92	0.54
$1s\,3d(^3D_3)$-$2p\,3d(^1F_3)$	2.4885	2.4867	2.40	1.80	1.22	0.80	15.10	15.70	1.17	0.57
$1s\,3d(^1D_2)$-$2p\,3d(^1F_3)$	2.4886	2.4868	2.40	1.80	8.95	8.20	15.10	15.70	8.60	5.89
$1s\,3p(^3P_1)$-$2p\,3p(^1D_2)$	2.4888	2.4868	11.10	8.97	0.19	0.19	12.95	13.02	0.44	0.38
$1s\,3p(^3P_2)$-$2p\,3p(^1D_2)$	2.4898	2.4878	11.10	8.97	1.22	0.92	13.00	13.09	2.81	1.87
$1s\,3d(^3D_1)$-$2p\,3d(^3P_1)$	2.4910		0.63		8.77		14.36		0.11	
$1s\,3s(^1S_0)$-$2p\,3s(^1P_1)$	2.4917	2.4897	8.58	6.17	8.24	6.93	11.40	10.60	10.60	7.63
$1s\,3p(^1P_1)$-$2p\,3p(^1D_2)$	2.4919	2.4899	11.10	8.97	8.94	8.63	13.00	13.00	20.60	17.60
$1s\,3p(^3P_1)$-$2p\,3p(^3P_2)$	2.4926	2.4908	0.02	0.13	5.29	5.28	15.73	15.43	0.03	0.21
$1s\,3d(^3D_2)$-$2p\,3d(^3D_3)$	2.4928	2.4912	0.16	0.96	6.26	4.81	14.99	15.06	0.47	0.21
$1s\,3s(^1S_0)$-$2p\,3d(^3D_1)$		2.4913		0.76		1.06		14.53		0.16
$1s\,3d(^3D_3)$-$2p\,3d(^3D_3)$	2.4932	2.4916	0.16	0.10	8.09	7.93	15.02	15.06	0.61	0.35
$1s\,3p(^3P_2)$-$2p\,3p(^3P_2)$	2.4936	2.4918	0.02	0.13	6.90	6.76	15.63	15.43	0.04	0.27
$1s\,3s(^3S_1)$-$2p\,3s(^3P_2)$	2.4938	2.4922	0.13	0.17	11.90	8.96	14.90	13.40	0.53	0.58
$1s\,3s(^3S_1)$-$2p\,3d(^3F_2)$		2.4925		0.26		3.20		13.29		0.31
$1s\,3d(^3D_2)$-$2p\,3d(^3D_2)$	2.4939		0.06		5.47		14.84		0.11	
$1s\,3d(^3D_1)$-$2p\,3d(^3D_2)$	2.4939		0.06		4.87		14.83		0.10	
$1s\,3d(^3D_3)$-$2p\,3d(^3D_2)$	2.4943		0.06		3.64		14.86		0.08	
$1s\,3p(^3P_1)$-$2s\,3d(^1D_2)$	2.4945	2.4935	3.05	2.13	4.58	2.89	8.09	6.08	6.27	3.74
$1s\,3d(^3D_2)$-$2p\,3s(^1P_1)$		2.4927		6.17		0.18		10.64		0.20
$1s\,3d(^3D_1)$-$2p\,3s(^1P_1)$	2.4946	2.4927	8.58	6.17	7.97	1.06	11.30	10.60	1.03	1.17
$1s\,3p(^3P_2)$-$2p\,3p(^3D_3)$	2.4947	2.4936	0.18	0.15	10.30	9.32	14.40	11.84	0.97	0.81
$1s\,3d(^1D_2)$-$2p\,3s(^1P_1)$	2.4951	2.4932	8.58	6.17	0.26	0.56	11.30	10.60	0.34	0.62
$1s\,3d(^3D_3)$-$2p\,3d(^3F_4)$	2.4953	2.4942	0.53	0.41	15.00	13.10	15.00	13.10	4.64	3.58
$1s\,3d(^3D_1)$-$2p\,3d(^3D_1)$	2.4963	2.4943	0.54	0.76	5.12	4.26	14.60	14.50	0.55	0.64
$1s\,3d(^3D_2)$-$2p\,3d(^3D_1)$	2.4963	2.4943	0.54	0.76	8.38	7.27	14.60	14.50	0.90	1.09
$1s\,3p(^3P_2)$-$2s\,3d(^1D_2)$		2.4946		2.13		0.30		6.07		0.38
$1s\,3p(^3P_1)$-$2s\,3d(^3D_1)$	2.4964		0.20		1.38		5.50		0.15	
$1s\,3s(^3S_1)$-$2p\,3s(^3P_1)$	2.4964	2.4949	0.50	0.39	8.66	10.40	11.10	11.90	1.12	0.99
$1s\,3p(^3P_1)$-$2p\,3d(^3D_2)$		2.4951		1.80		0.36		6.02		0.42
$1s\,3p(^3P_1)$-$2p\,3d(^3P_0)$	2.4966		0.25		13.7		17.34		0.19	
$1s\,3p(^3P_2)$-$2s\,3d(^3D_2)$	2.4974	2.4961	2.41	1.80	2.21	1.95	5.83	6.02	3.23	2.24
$1s\,3p(^3P_2)$-$2p\,3d(^3D_1)$	2.4974	2.4962	0.20	0.17	2.81	2.04	5.50	6.29	0.30	0.16
$1s\,3d(^1D_2)$-$2p\,3d(^1D_2)$	2.4975	2.4960	0.04	0.05	9.43	8.93	14.34	13.61	0.13	0.15
$1s\,2p(^1P_1)$-$2s\,3d(^1D_2)$	2.4976	2.4967	3.05	2.13	1.77	1.37	8.08	6.08	2.43	1.77
$1s\,3s(^3S_1)$-$2s\,3p(^3P_0)$	2.4979	2.4975	0.12	0.57	4.88	3.01	8.32	5.79	0.07	0.27
$1s\,3d(^3D_2)$-$2p\,3d(^3F_3)$	2.4985	2.4968	0.58	0.43	3.82	4.16	1.49	13.30	1.00	0.91
$1s\,3s(^3S_1)$-$2s\,3p(^3P_1)$	2.4985	2.4970	0.90	0.59	3.30	1.27	6.70	4.85	1.17	0.41
$1s\,3d(^3D_3)$-$2p\,3d(^3F_3)$	2.4989	2.4972	0.58	0.43	5.66	4.47	14.88	13.34	1.47	0.97
$1s\,3d(^1D_2)$-$2p\,3d(^3F_3)$	2.4990	2.4973	0.58	0.43	5.41	4.45	14.88	13.34	1.41	0.97
$1s\,3p(^3P_2)$-$2s\,3d(^3D_3)$	2.4992	2.4982	0.07	0.05	4.65	3.93	5.84	6.83	0.40	0.22
$1s\,3s(^3S_1)$-$2p\,3s(^3P_0)$	2.4993		0.56		9.78		11.12		0.47	
$1s\,3p(^1P_1)$-$2s\,3d(^3D_2)$	2.4995	2.4982	2.41	1.80	2.40	2.16	5.81	6.02	3.52	2.49
$1s\,3d(^3D_1)$-$2p\,3s(^3P_2)$		2.4985		0.18		2.33		13.43		0.15
$1s\,3p(^3P_1)$-$2p\,3p(^3D_2)$	2.5004	2.4990	0.62	0.27	4.87	4.53	13.79	12.52	1.04	0.48
$1s\,3d(^3D_1)$-$2p\,3d(^3F_2)$	2.5006	2.4987	0.40	0.26	7.76	5.37	14.82	13.29	1.01	0.52
$1s\,3d(^3D_1)$-$2p\,3d(^3F_2)$	2.5006	2.4988	0.40	0.26	5.85	4.19	14.80	13.30	0.76	0.40
$1s\,3p(^3P_2)$-$2p\,3p(^3D_2)$	2.5014	2.5000	0.62	0.27	4.51	3.25	13.80	12.50	0.96	0.34
$1s\,3p(^3P_1)$-$2s\,3s(^1S_0)$	2.5032	2.5019	16.40	12.90	1.17	0.65	4.16	3.29	0.94	0.52
$1s\,3p(^1P_1)$-$2p\,3p(^3D_2)$	2.5035		0.62		1.59		13.84		0.34	
$1s\,3d(^3D_3)$-$2s\,3p(^3P_2)$	2.5041	2.5030	0.59	0.46	1.44	1.30	5.29	4.61	0.72	0.59
$1s\,3d(^3D_2)$-$2p\,3p(^3P_1)$		2.5034		0.59		0.50		4.85		0.16
$1s\,3s(^1S_0)$-$2s\,3p(^1P_1)$	2.5048	2.5034	0.10	0.14	5.65	4.80	9.83		0.17	0.23
$1s\,3p(^1P_1)$-$2s\,3s(^1S_0)$	2.5064	2.5051	16.40	12.90	2.15	2.08	4.27	3.29	1.71	1.66
$1s\,3p(^3P_2)$-$2p\,3s(^3S_1)$	2.5077		0.07		1.92		3.89		0.11	

TABLE III. Atomic data for satellites of the Ti XXII resonance line due to transitions $1s\,4l$-$2l'4l''$ from the Z-expansion method (superscript 1) and from SUPERSTRUCTURE (superscript 2). Wavelengths are in Å. Radiative probability A_r, autoionization probability A_a, and line factors $F_2(s)$ are in 10^{13} s^{-1}.

Array	λ^1	λ^2	A_a^1	A_a^2	A_r^1	A_r^2	$\sum A_r^1$	$\sum A_r^2$	$F_2^1(s)$	$F_2^2(s)$
$1s\,4p\,(^1P_1)$-$2p\,4p\,(^1S_0)$	2.4896	2.4883	1.07	0.84	13.40	11.94	15.57	13.80	0.87	0.69
$1s\,4d\,(^3D_2)$-$2p\,4d\,(^1F_3)$	2.4896	2.4885	0.90	0.84	4.82	4.03	15.10	14.10	1.90	1.58
$1s\,4f\,(^1F_3)$-$2p\,4f\,(^3D_2)$		2.4885		0.05		13.03		13.59		0.26
$1s\,4d\,(^3D_3)$-$2p\,4d\,(^1F_3)$	2.4898	2.4886	0.90	0.84	2.78	2.39	15.10	14.10	1.10	0.94
$1s\,4d\,(^1D_2)$-$2p\,4d\,(^1F_3)$	2.4898	2.4887	0.90	0.84	7.45	6.76	15.10	14.10	2.94	2.65
$1s\,4f\,(^3F_3)$-$2p\,4f\,(^1G_4)$		2.4888		0.04		10.10		13.42		0.24
$1s\,4s\,(^3S_1)$-$2p\,4s\,(^1P_1)$	2.4903	2.4889	2.90	1.97	2.58	2.40	13.12	11.87	1.40	1.03
$1s\,4f\,(^3F_2)$-$2p\,4f\,(^1D_2)$		2.4890		0.04		8.81		13.56		0.13
$1s\,4f\,(^3F_4)$-$2p\,4f\,(^3G_5)$		2.4891		0.02		13.15		13.43		0.26
$1s\,4p\,(^3P_2)$-$2p\,4p\,(^1D_2)$	2.4907	2.4893	4.72	3.37	4.39	3.62	15.99	13.97	4.99	3.51
$1s\,4d\,(^3D_1)$-$2p\,4d\,(^3P_1)$	2.4908		0.03		10.8		14.77		0.06	
$1s\,4d\,(^3D_2)$-$2p\,4d\,(^3D_3)$	2.4915	2.4900	0.12	0.10	8.82	7.85	15.01	13.74	0.47	0.38
$1s\,4p\,(^1P_1)$-$2p\,4p\,(^1D_2)$	2.4916	2.4901	4.72	3.37	9.83	8.57	16.06	13.97	11.20	8.32
$1s\,4s\,(^3S_1)$-$2p\,4d\,(^3P_2)$	2.4916		0.05		13.6		14.92		0.21	
$1s\,4d\,(^3D_3)$-$2p\,4d\,(^3D_3)$	2.4917	2.4902	0.12	0.01	5.21	4.44	15.03	13.74	0.28	0.21
$1s\,4p\,(^3P_1)$-$2p\,4p\,(^3P_2)$	2.4917	2.4901	0.99	0.54	11.50	10.35	16.35	14.31	3.28	1.87
$1s\,4f\,(^3F_2)$-$2p\,4p\,(^1D_2)$		2.4902		3.37		0.10		13.97		0.10
$1s\,4f\,(^1F_3)$-$2p\,4p\,(^1D_2)$		2.4903		3.37		0.17		13.97		0.17
$1s\,4s\,(^1S_0)$-$2p\,4s\,(^1P_1)$	2.4918	2.4903	2.90	1.97	10.00	8.96	13.07	11.90	5.44	3.83
$1s\,4d\,(^3D_2)$-$2p\,4d\,(^1D_2)$	2.4920		0.04		4.52		14.98		0.06	
$1s\,4d\,(^3D_1)$-$2p\,4d\,(^1D_2)$	2.4920		0.04		4.89		14.95		0.07	
$1s\,4p\,(^3P_2)$-$2p\,4p\,(^3P_2)$	2.4921	2.4905	0.99	0.54	2.58	2.31	16.33	14.31	0.73	0.42
$1s\,4d\,(^1D_2)$-$2p\,4d\,(^1D_2)$	2.4922		0.04		3.49		15.00		0.05	
$1s\,4d\,(^3D_3)$-$2p\,4d\,(^3F_4)$	2.4924	2.4906	0.23	0.20	15.00	12.90	15.00	13.05	2.00	1.74
$1s\,4p\,(^3P_2)$-$2p\,4p\,(^3D_3)$	2.4926	2.4908	0.04	0.04	14.30	12.68	16.09	14.00	0.22	0.27
$1s\,4d\,(^3D_1)$-$2p\,4s\,(^1P_1)$		2.4915		1.97		0.24		11.87		0.10
$1s\,4p\,(^3P_1)$-$2s\,4d\,(^1D_2)$	2.4945		0.03		0.92		2.23		0.07	
$1s\,4p\,(^3P_2)$-$2s\,4d\,(^1D_2)$	2.4949	2.4951	0.03	0.70	1.01	1.32	2.23	4.40	0.07	0.91
$1s\,4s\,(^3S_1)$-$2p\,4s\,(^3P_1)$	2.4953	2.4935	1.14	0.81	6.89	7.74	8.29	9.18	2.50	1.88
$1s\,4p\,(^3P_1)$-$2p\,4p\,(^3P_0)$	2.4957		0.14		12.60		14.23		0.12	
$1s\,4p\,(^3P_1)$-$2s\,4d\,(^3D_1)$	2.4960		0.09		1.11		2.25		0.07	
$1s\,4p\,(^3P_2)$-$2s\,4d\,(^3D_2)$	2.4964	2.4958	0.71	0.25	1.86	1.21	4.25	5.40	1.33	0.27
$1s\,4p\,(^3P_2)$-$2s\,4d\,(^3D_1)$	2.4964		0.09		2.46		4.41		0.146	
$1s\,4d\,(^3D_3)$-$2p\,4d\,(^3D_2)$	2.4964		0.02		8.29		13.87		0.06	
$1s\,4d\,(^3D_2)$-$2p\,4d\,(^3F_3)$	2.4965	2.4940	0.31	0.23	1.38	0.69	14.99	10.09	0.20	0.11
$1s\,4d\,(^3D_3)$-$2p\,4d\,(^3F_3)$	2.4967	2.4942	0.31	0.23	6.98	4.95	14.93	10.09	0.99	0.77
$1s\,4d\,(^1D_2)$-$2p\,4d\,(^3F_3)$	2.4967	2.4943	0.31	0.23	6.56	4.04	14.95	10.09	0.93	0.63
$1s\,4p\,(^1P_1)$-$2s\,4d\,(^1D_2)$		2.4960		0.70		2.30		4.40		1.59
$1s\,4s\,(^1S_0)$-$2p\,4s\,(^3P_1)$		2.4948		0.81		0.55		9.18		0.13
$1s\,4d\,(^3D_3)$-$2s\,4f\,(^3F_3)$		2.4953		0.06		1.43		3.79		0.16
$1s\,4d\,(^1D_2)$-$2s\,4f\,(^3F_3)$		2.4954		0.06		1.47		3.79		0.16
$1s\,4s\,(^3S_1)$-$2s\,4p\,(^3P_1)$	2.4967	2.4956	0.41	0.29	1.24	1.10	3.54	2.73	0.38	0.31
$1s\,4p\,(^3P_2)$-$2s\,4d\,(^3D_3)$	2.4968	2.4958	0.07	0.06	0.68	0.53	0.76	1.50	0.40	0.15
$1s\,4s\,(^3S_1)$-$2p\,4s\,(^3P_0)$	2.4972	2.4959	0.23	0.21	10.2	3.32	10.80	4.41	0.21	0.15
$1s\,4p\,(^3P_2)$-$2s\,4d\,(^3D_2)$		2.4962		0.25		1.98		5.40		0.44
$1s\,4p\,(^1P_1)$-$2s\,4d\,(^3D_2)$	2.4973	2.4971	0.71	0.25	1.77	1.06	4.25	5.40	1.26	0.24
$1s\,4p\,(^3P_1)$-$2p\,4p\,(^3D_2)$	2.4974	2.4935	0.80	0.22	2.38	1.46	11.66	7.02	0.76	0.22
$1s\,4d\,(^3D_2)$-$2p\,4d\,(^3F_2)$	2.4977	2.4957	0.18	0.09	6.63	3.85	14.82	9.19	0.39	0.21
$1s\,4d\,(^3D_1)$-$2p\,4d\,(^3F_2)$	2.4977	2.4957	0.18	0.09	8.02	5.01	14.81	9.19	0.48	0.27
$1s\,4p\,(^3P_2)$-$2p\,4p\,(^3D_2)$	2.4978	2.4940	0.80	0.22	5.13	3.91	11.70	7.02	1.64	0.58
$1s\,4s\,(^3S_1)$-$2s\,4p\,(^1P_1)$	2.4979	2.4962	0.06	0.19	4.03	1.86	11.71	6.62	0.79	0.16
$1s\,4p\,(^1P_1)$-$2p\,4p\,(^3P_1)$	2.4979		0.01		4.47		12.44		0.01	
$1s\,4p\,(^1P_1)$-$2p\,4p\,(^3D_2)$	2.4987	2.4948	0.80	0.22	2.89	0.71	11.71	7.02	0.92	0.11
$1s\,4p\,(^3P_1)$-$2s\,4s\,(^1S_0)$	2.4987	2.4978	6.49	4.67	1.94	0.82	3.94	2.40	1.21	0.54
$1s\,4d\,(^3D_3)$-$2s\,4p\,(^3P_2)$	2.4991	2.4980	0.23	0.20	1.49	0.99	3.51	2.46	0.45	0.36
$1s\,4s\,(^1S_0)$-$2s\,4p\,(^1P_1)$	2.4993	2.4975	0.06	0.19	4.51	3.30	9.74	6.62	0.09	0.28
$1s\,4d\,(^3D_2)$-$2s\,4p\,(^3P_1)$	2.4994	2.4982	0.41	0.29	0.56	0.48	3.54	2.73	0.17	0.14
$1s\,4p\,(^1P_1)$-$2s\,4s\,(^1S_0)$	2.5001	2.4991	6.49	4.67	1.56	1.35	3.91	2.40	0.97	0.89
$1s\,4p\,(^3P_2)$-$2s\,4s\,(^3S_1)$	2.5005		0.03		1.79		3.04		0.05	

TABLE IV. Atomic data for satellites of the Ti XXII resonance line due to transitions $1s\,5l$-$2l'5l''$ from the Z-expansion method (superscript 1) and from SUPERSTRUCTURE (superscript 2). Wavelengths are in Å. Radiative probability A_r, autoionization probability A_a, and line factors $F_2(s)$ are in 10^{13} s^{-1}.

Array	λ^1	λ^2	A_a^1	A_a^2	A_r^1	A_r^2	$\sum A_r^1$	$\sum A_r^2$	$F_2^1(s)$	$F_2^2(s)$
$1s\,5d\,(^3D_2)$-$2p\,5d\,(^1F_3)$	2.4900	2.4888	0.42	0.42	4.60	3.87	15.07	13.61	0.87	0.81
$1s\,5f\,(^1F_3)$-$2p\,5f\,(^1D_2)$		2.4888		0.03		13.09		13.43		0.13
$1s\,5f\,(^3F_3)$-$2p\,5f\,(^1G_4)$		2.4889		0.03		9.63		13.32		0.18
$1s\,5d\,(^3D_3)$-$2p\,5d\,(^1F_3)$	2.4901	2.4889	0.42	0.42	3.91	3.39	15.04	13.61	0.74	0.71
$1s\,5d\,(^1D_2)$-$2p\,5d\,(^1F_3)$	2.4901	2.4889	0.42	0.42	6.54	5.94	15.04	13.60	1.24	1.25
$1s\,5p\,(^1P_1)$-$2p\,5p\,(^1S_0)$	2.4902	2.4889	0.75	0.53	13.50	11.98	15.55	13.64	0.62	0.45
$1s\,5f\,(^3F_4)$-$2p\,5f\,(^3G_5)$		2.4891		0.02		13.18		13.32		0.20
$1s\,5p\,(^3P_2)$-$2p\,5p\,(^1D_2)$	2.4906	2.4892	2.12	1.42	5.86	4.99	15.90	13.65	3.45	2.35
$1s\,5s\,(^3S_1)$-$2p\,5s\,(^1P_1)$	2.4906	2.4892	1.07	0.68	3.93	3.66	14.40	12.86	0.82	0.56
$1s\,5d\,(^3D_2)$-$2p\,5d\,(^3D_3)$	2.4910	2.4895	0.69	0.58	9.85	8.72	15.04	13.46	0.32	0.26
$1s\,5s\,(^3S_1)$-$2p\,5s\,(^3P_2)$	2.4910		0.03		14.50		14.97		0.14	
$1s\,5p\,(^1P_1)$-$2p\,5p\,(^1D_2)$	2.4911	2.4897	2.12	1.42	9.03	7.79	15.90	13.65	5.31	3.67
$1s\,5d\,(^3D_3)$-$2p\,5d\,(^3D_3)$	2.4911	2.4896	0.69	0.06	4.01	3.52	15.06	13.46	0.13	0.11
$1s\,5p\,(^3P_1)$-$2p\,5p\,(^3P_2)$	2.4911	2.4896	0.64	0.31	13.00	11.60	15.94	13.72	2.51	1.30
$1s\,5s\,(^1S_0)$-$2p\,5s\,(^1P_1)$	2.4913	2.4898	1.07	0.68	10.20	9.02	14.41	12.86	2.11	1.37
$1s\,5p\,(^3P_2)$-$2p\,5p\,(^3P_2)$	2.4913	2.4898	0.64	0.31	1.24	1.18	16.00	13.72	0.24	0.13
$1s\,5d\,(^3D_3)$-$2p\,5d\,(^3F_4)$	2.4914	2.4898	0.12	0.10	15.00	13.11	15.00	13.20	1.03	0.92
$1s\,5p\,(^3P_2)$-$2p\,5p\,(^3D_3)$	2.4916	2.4898	0.01	0.02	14.9	13.11	15.92	13.66	0.08	0.12
$1s\,5s\,(^1S_0)$-$2p\,5s\,(^3P_1)$		2.4942		0.56		2.07		9.74		0.34
$1s\,5p\,(^3P_1)$-$2s\,5d\,(^1D_2)$	2.4950		0.04		0.33		1.46		0.05	
$1s\,5p\,(^3P_2)$-$2s\,5d\,(^1D_2)$	2.4952	2.4949	0.04	0.12	0.92	0.65	1.46	2.14	0.14	0.18
$1s\,5s\,(^3S_1)$-$2s\,5p\,(^1P_1)$	2.4953	2.4952	0.98	0.22	5.00	1.65	6.40	4.39	1.99	0.23
$1s\,5p\,(^1P_1)$-$2s\,5d\,(^1D_2)$		2.4953		0.12		0.12		2.14		0.31
$1s\,5p\,(^3P_1)$-$2p\,5p\,(^3P_0)$	2.4955		0.06		11.30		12.46		0.06	
$1s\,5s\,(^1S_0)$-$2s\,5p\,(^1P_1)$	2.4960	2.4958	0.98	0.22	0.56	1.93	6.40	4.39	0.22	0.27
$1s\,5p\,(^3P_2)$-$2s\,5d\,(^3D_2)$	2.4960	2.4954	0.32	0.07	1.78	0.69	3.82	1.87	0.69	0.13
$1s\,5p\,(^3P_2)$-$2s\,5d\,(^3D_1)$	2.4960		0.05		2.44		4.14		0.08	
$1s\,5d\,(^3D_3)$-$2p\,5d\,(^3F_3)$	2.4961	2.4939	0.19	0.19	7.08	6.03	14.94	12.70	0.62	0.61
$1s\,5d\,(^1D_2)$-$2p\,5d\,(^3F_3)$	2.4961	2.4939	0.19	0.19	7.27	5.93	14.92	12.70	0.64	0.60
$1s\,5p\,(^3P_2)$-$2p\,5d\,(^3D_3)$	2.4962		0.41		0.14		0.15		0.21	
$1s\,5s\,(^3S_1)$-$2s\,5p\,(^3P_1)$	2.4962	2.4951	0.21	0.14	0.66	0.43	2.25	1.25	0.17	0.13
$1s\,5s\,(^3S_1)$-$2p\,5s\,(^3P_0)$	2.4965		0.11		10.50		10.81		0.11	
$1s\,5p\,(^1P_1)$-$2s\,5d\,(^3D_2)$	2.4965		0.32		1.61		3.84		0.63	
$1s\,5p\,(^3P_1)$-$2p\,5p\,(^3D_2)$	2.4965	2.4937	0.58	0.50	1.49	1.19	10.97	10.54	0.37	0.27
$1s\,5d\,(^3D_2)$-$2p\,5d\,(^3F_2)$	2.4967	2.4943	0.09	0.07	6.93	5.24	14.78	10.99	0.21	0.16
$1s\,5d\,(^3D_1)$-$2p\,5d\,(^3F_2)$	2.4967	2.4943	0.09	0.07	7.72	5.40	14.78	10.99	0.23	0.17
$1s\,5p\,(^3P_2)$-$2p\,5p\,(^3D_2)$	2.4967	2.4939	0.58	0.50	5.18	5.62	11.00	10.54	1.30	1.26
$1s\,5s\,(^3S_1)$-$2p\,5s\,(^3P_1)$	2.4968	2.4936	0.04	0.56	5.22	7.41	9.96	9.74	0.06	1.21
$1s\,5p\,(^1P_1)$-$2p\,5p\,(^3D_2)$	2.4972	2.4943	0.58	0.50	3.56	3.18	10.94	10.50	0.90	0.71
$1s\,5p\,(^3P_1)$-$2p\,5p\,(^1S_0)$	2.4972		3.14		2.59		4.03		1.13	
$1s\,5p\,(^3P_1)$-$2s\,5s\,(^1S_0)$		2.4962		1.99		0.71		1.58		0.40
$1s\,5d\,(^3D_3)$-$2s\,5p\,(^3P_2)$	2.4974	2.4963	0.11	0.09	1.45	0.63	2.79	1.24	0.28	0.21
$1s\,5d\,(^3D_2)$-$2s\,5p\,(^3P_1)$		2.4964		0.14		0.35		1.25		0.11
$1s\,5p\,(^1P_1)$-$2s\,5s\,(^1S_0)$		2.4969		1.99		0.80		1.58		0.44
$1s\,5d\,(^3D_2)$-$2s\,5p\,(^3P_1)$	2.4975		0.22		0.56		2.24		0.15	
$1s\,5p\,(^1P_1)$-$2p\,5p\,(^1S_0)$	2.4979		3.14		1.19		4.07		0.52	

tio of two has been assumed for the fine-structure components of the Ti XXII resonance line, since excitation of the $2P_{3/2}$ and the $2P_{1/2}$ states from the $2S_{1/2}$ state by proton collisions are negligible at the plasma densities obtained in PLT discharges.[27] The theoretical spectrum also includes the contribution of the magnetic dipole transition from $2S_{1/2}$ to $1S_{1/2}$. This transition is not strictly forbidden,[35] although the dominant decay of the $2S_{1/2}$ state is a two-photon process. Rate coefficients for the magnetic dipole transition ($M1$) and the two-photon ($2E1$) decay of the $2S_{1/2}$ state have been derived by Breit and Teller[36] and Drake,[37] who obtained the following results:

$$A_{M1}=2.496\times10^{-6}Z^{10}\ \text{s}^{-1}\ ,$$

$$A_{2E1}=8.228Z^{6}\ \text{s}^{-1}\ .$$

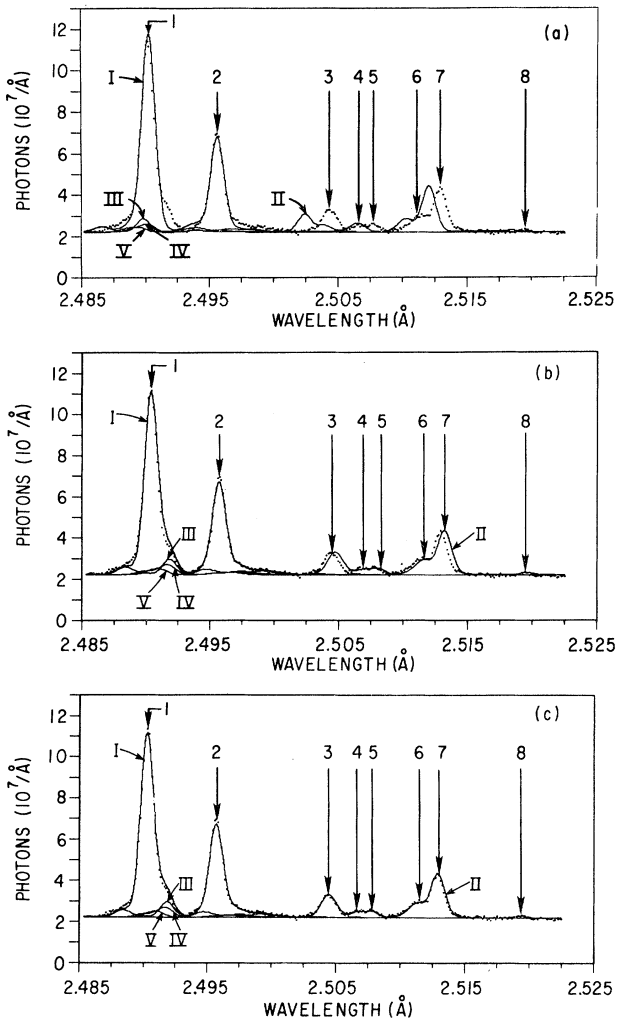

FIG. 6. Experimental Ti XXII data and theoretical predictions (solid lines) (a) from SUPERSTRUCTURE and (b) from the Z-expansion method. Curves II—V and curve I represent the contributions from dielectronic satellites with $n=2$—5 and the total intensity which includes the contribution from the Ly-α lines (features 1 and 2). Also included in the theoretical spectra is the contribution from the $2S_{1/2}$-$1S_{1/2}$ magnetic dipole transition. (c) shows the experimental data and a synthetic spectrum which has been obtained from the Z-expansion data after a slight correction of the theoretical wavelengths of all the $n=2$ satellites by the same amount of 0.0003 Å and using a value of 2.4903 Å (instead of Safronova's value of 2.4904 Å) for the wavelength of the Ly-α_1 line.

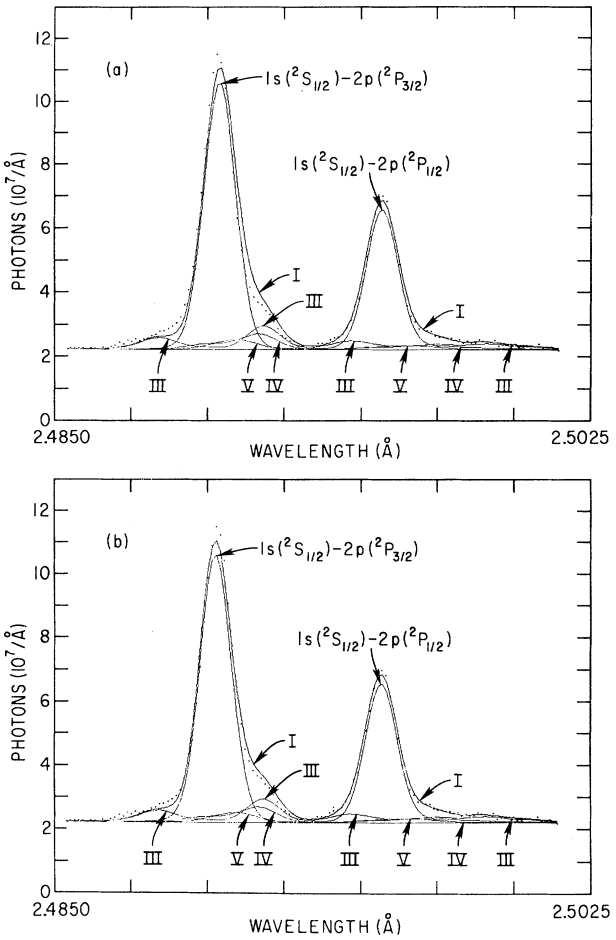

FIG. 7. Spectrum of the Ly-α lines and associated $n \geq 3$ satellites from Figs. 6(b) and 6(c) on an enlarged scale.

Because of the different Z dependences of these decay processes, the $M1$ transition becomes important for ions with $Z \geq 20$. The intensity ratio of the $M1$ line and the Ly-α_2 line is given by the expression

$$\frac{I(M1)}{I(\text{Ly-}\alpha_2)} = c\frac{A(M1)}{A(M1)+A(2E1)} , \tag{1}$$

where $c=0.63$ (for $T_e=2$ keV) is the ratio of the excitation rates of the $2S_{1/2}$ and the $2P_{1/2}$ states from the $1S_{1/2}$ ground state.[31] From this expression we obtain for $I(M1)/I(\text{Ly-}\alpha_2)$ a value of 0.04. The $M1$ line is separated from the Ly-α_2 line by the Lamb shift, which is 0.164 mÅ for Ti XXII.[1] This value is small compared with the Doppler width ($\simeq$1 mÅ) and the $M1$ line is, therefore, not resolved in the observed Ti XXII spectrum.

The intensities i_d of the satellites relative to the intensity of the resonance line have been calculated from the expression given by Gabriel and Paget[38] for the zero density limit, assuming a Maxwellian energy distribution for the electrons,

$$i_d = \frac{2.619\times10^{-14}}{T_e^{3/2}C_R(T_e)}\exp\left[\frac{-E_s^{(n)}}{T_e}\right]F_2(s) , \tag{2}$$

where T_e is the electron temperature in keV. $E_s^{(n)}$(=3.4, 4.3, 4.6, and 4.7 keV, for $n=2$, 3, 4, and 5) is the average energy of the autoionizing heliumlike states of a given n-shell relative to the hydrogenlike ground state. The line factor $F_2(s)$ for the satellite line s: $\gamma\rightarrow\gamma'$ (between the heliumlike ion levels γ and γ') is defined as

$$g_s \frac{A_a(s)A_r(s)}{A_a(s)+\sum_{s'} A_r(s')} ,$$

where g_s is the statistical weight of the doubly excited heliumlike state γ. $A_a(s)$ is the probability for autoionization of the state γ to the hydrogenlike ground state $1s$. $A_r(s)$ is the probability for the stabilizing radiative transition s and $\sum_{s'} A_r(s')$ is the total radiative decay probability for the state γ. $A_r(s)$, $A_a(s)$, and $F_2(s)$ are in units of 10^{13} s^{-1}. $C_r(T_e)$ is the excitation rate for the total Ti XXII resonance transition $1s$-$2p$. Safronova, Urnov, and Vainshtein obtained the following expression for $C_R(T_e)$ from a fit of their Coulomb-Born calculations:[31]

$$C_R(T_e)=\frac{3.37\times10^{-11}}{E_0 T_e^{1/2}}\exp\left[\frac{-E_0}{T_e}\right]\frac{1+E_0/T_e}{0.24+E_0/T_e} , \quad (3)$$

where $E_0=4.94$ keV is the energy of the Ti XXII resonance transition. Faucher and Volonte[39] have determined $C_R(T_e)$ from distorted-wave calculations and included corrections for radiative cascades from $n\geq3$ following the method described by Bely-Dubau *et al.*[40] For the electron temperatures of interest, their values are larger by only 10% than those obtained from Eq. (3), e.g., for $T_e=2.1$ keV the values are 6.5×10^{-13} and 5.8×10^{-13} cm^{3}s^{-1}. Since this 10% correction is within the experimental error, we use Eq. (3) in the following part of this work.

Figures 6(a) and 6(b) show the experimental data and the synthetic spectra for the results obtained from SUPERSTRUCTURE and the Z-expansion method, respectively. In order to obtain a best fit with the experimental data, the ion and electron temperatures were chosen to be $T_i=1.8$ keV and $T_e=2.1$ keV. The theoretical spectra are in very good agreement with the experimental data. This is true, in particular, for the relative intensities of the satellites and resonance line. Only small discrepancies are observed between theoretical and experimental wavelengths. These discrepancies are larger for the data of Dubau *et al.* ($\simeq$0.0009 Å) than for those of Safronova and Vainshtein ($\simeq$0.0003 Å). The almost perfect fit shown in Fig. 6(c) has been obtained by reducing the theoretical wavelengths of Safronova and Vainshtein for the $n=2$ satellites by the constant amount of 0.0003 Å and using the value of 2.4903 Å (instead of Safronova's value of 2.4904 Å) for the wavelength of the Ly-α_2 line.

Figures 7(a) and 7(b) present the spectral range from 2.4850 to 2.5025 Å of Figs. 6(b) and 6(c) on an enlarged scale to allow for a more detailed comparison of the theoretical predictions for the fine-structure components of the Ti XXII resonance line and their associated $n\geq3$ satellites with the experimental data. The predicted (apparent) intensity profile of the Ly-α_2 line is in excellent agreement with the observation. However, a small discrepancy between theory and experiment is observed on the long wavelength side of the Ly-α_1 line in Fig. 7(a). In Fig. 7(b) this discrepancy has been largely removed by increasing the separation of the fine-structure components by 0.1 mÅ. We thus obtain the value of 0.0054 Å for this separation which, as mentioned before, is in good agreement with the theoretical predictions of Erickson[1] and Safronova and Shestakov.[32]

IV. DIAGNOSTIC APPLICATIONS

The satellite spectra of hydrogenlike ions are important for the diagnosis of hot plasmas. The main diagnostic applications are measurements of the ion and electron temperatures, which can be determined from the Doppler broadening of spectrum lines and from the relative intensities of the resonance line and the associated dielectronic satellites. Of particular interest are the spectra of hydrogenlike ions with $Z\geq20$ for measurements of the central ion temperature in the next generation of large tokamaks with expected core ion and electron temperatures in excess of 10 keV. Under these conditions impurity ions with $Z\leq20$ will be fully stripped in the hot center of the plasma, whereas ions with $Z\geq20$ will predominantly be in the hydrogenlike charge state. The ion temperature in the hot core of the plasma can thus be obtained from Doppler-broadening measurements of the resonance lines of these ions. Doppler-broadening measurements of Ly-α lines may indeed be the most important central-ion-temperature diagnostic for these tokamaks since determination of the central ion temperature by standard techniques, such as the measurement of charge exchange neutrals, will be prevented by the projected large plasma densities and plasma radii. The ion and electron temperature results, which we obtained from evaluation of the Ti XXII spectra, are shown in Figs. 8 and 9.

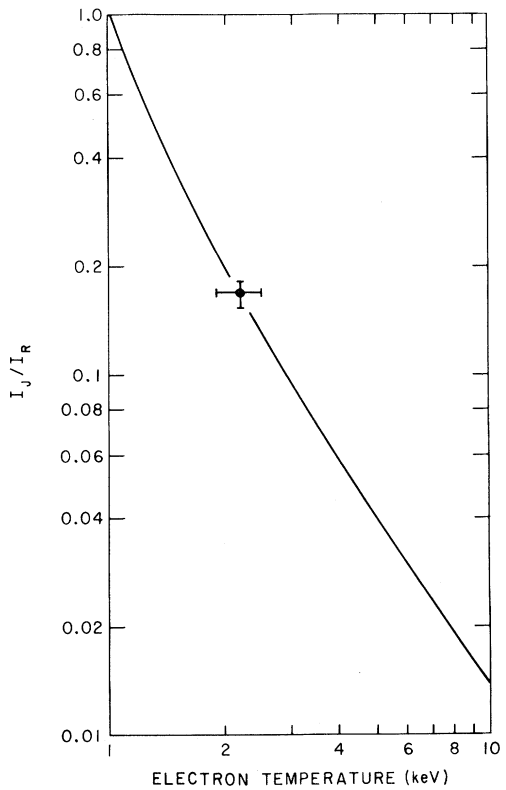

FIG. 8. Intensity of the satellite J relative to the total resonance-line intensity from the spectrum in Fig. 4 vs the experimental value of the central electron temperature. Also shown is the electron-temperature dependence (solid line) predicted by Eqs. (2) and (3).

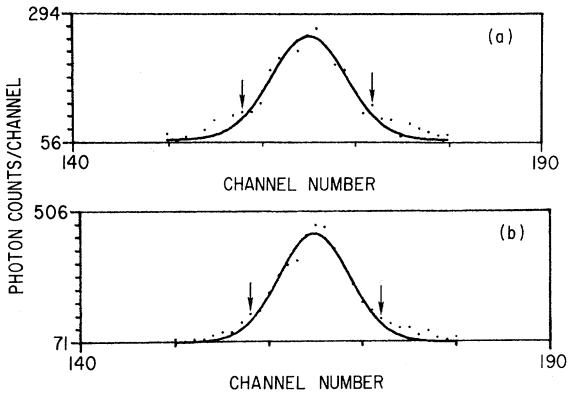

FIG. 9. Least-squares fits of single Voigt functions (solid lines) to the line profiles of Ly-α_2 from the spectra in Figs. 2(a) and 2(b). The arrows indicate the range used for the fit. The ion-temperature values obtained from these fits are $T_i=2.0\pm0.2$ keV [for (a)] and $T_i=1.8\pm0.1$ keV [for (b)].

Figure 8 presents the satellite-to-resonance-line ratio I_J/I_R for the most prominent satellite J from the spectrum in Fig. 4 versus the experimental value of the central electron temperature (obtained from laser Thomson scattering data) and, for comparison, the theoretical electron temperature dependence given by Eqs. (2) and (3). The theory and the observations are in agreement to within the experimental errors. According to the theoretical predictions, the ratio I_J/I_R is very sensitive to the electron temperature (solid line in Fig. 8). We may conclude that I_J/I_R can be used as an electron-temperature diagnostic up to values of $T_e=3$ keV. For higher electron temperatures the ratio I_J/I_R is smaller than 10% and it will be difficult to measure I_J/I_R with sufficient accuracy.

The ion temperature has been determined from the observed line profile of Ly-α_2. As discussed in Sec. III this line profile also includes the contribution from the $n\geq3$ satellites which are associated with the $1s(^2S_{1/2})$-$2p(^2P_{1/2})$ transition. In principle, the ion temperature has, therefore, to be evaluated from a fit of a synthetic spectrum, which includes the contribution from these satellites, with the experimental data. However, the time needed for these computations prevents a fast ion-temperature determination which is desired in tokamak experiments. We, therefore, compared the ion-temperature results, which we derived from a fit of the complete line structure to the experimental data [e.g., see Fig. 7(b)], with those obtained from a single Voigt-function fit. Figure 9 shows least-squares fit of single Voigt profiles (solid lines) to the (apparent) Ly-α_2 line profiles of the spectra in Figs. 2(a) and 2(b). The Voigt profiles were calculated with use of the plasma dispersion function as described by Bitter *et al.*[21] The arrows indicate the limits of the spectral range which was used for the fit. The fitting limits have been chosen to exclude most of the wing structure which is determined by the relatively intense $n=3$ satellites. The ion-temperature values, obtained from a single Voigt-function fit to the data in Figs. 9(a) and 9(b), where $T_i=2.0\pm0.2$ and 1.8 ± 0.1 keV. These values are practically identical with the values obtained from the fit of the complete line structure. One can expect that the intensity of the $n\geq3$ satellites strongly decreases with increasing electron temperature and that the observed line profile will be very well approximated by a single Voigt profile if the electron temperature exceeds 3 keV.

V. DIELECTRONIC RECOMBINATION RATE COEFFICIENT

The total dielectronic recombination rate coefficient α_d can be written in the form[41,34]

$$\alpha_d=C_R(T_e)\sum_s I_s/I_R\ , \tag{4}$$

where $\sum_s I_s/I_R$ is the total intensity of all the dielectronic satellites relative to the intensity of the resonance line and $C_R(T_e)$ is the collision excitation rate coefficient for the resonance transition. The dielectronic recombination rate coefficient α_d can thus be experimentally determined from a measurement of the total relative satellite intensity $\sum_s I_s/I_R$ if the excitation rate coefficient $C_R(T_e)$ is known.

So far, this method has been used to determine the dielectronic recombination rate coefficients for the heliumlike charge states of calcium Ca XIX[42] and iron Fe XXV.[43] Satellites to the heliumlike resonance lines are due to transitions of the type $1s^2nl$-$1s2pnl$ with $n\geq2$. These satellites are produced by the process of dielectronic recombination as well as by collisional inner-shell excitation of lithiumlike ions in the $1s^22s$ ground state. Appropriate corrections for the latter contribution are, therefore, necessary for a measurement of the dielectronic recombination rate coefficient from lithiumlike satellites. This is different for the heliumlike $1snl$-$2pnl$ (with $n\geq2$) satellites of the hydrogenlike resonance lines since they are entirely produced in the process of dielectronic recombination. These satellites are, therefore, of principal importance for these measurements.

Figure 10 shows the experimental value of the dielectronic recombination rate coefficient α_d for hydrogenlike titanium Ti XXII. This rate coefficient has been obtained from the spectrum in Fig. 4 by multiplying the observed total relative satellite to resonance-line intensity $\sum_s I_s/I_R$ by the theoretical value for $C_R(T_e)$ which was calculated from Eq. (3). The experimental value of $\sum_s I_s/I_R$ includes the intensity contributions from all the $n=2$ satellites and from those $n=3$ satellites which can be resolved on the wings of the apparent Ly-α_1 and Ly-α_2 line profiles. A part of the $n=3$ satellites and all the $n\geq4$ satellites are blended with the Ly-α_1 and the Ly-α_2 lines so that their contribution cannot be directly measured. However, since the theoretical results for the $n=2$ and 3 satellites on the wings of the resonance lines are in very good agreement with the observation, we may assume that the predictions for the unresolved $n\geq3$ satellites are also reliable. With this assumption we estimated the intensity contribution from unresolved satellites to α_d. This contri-

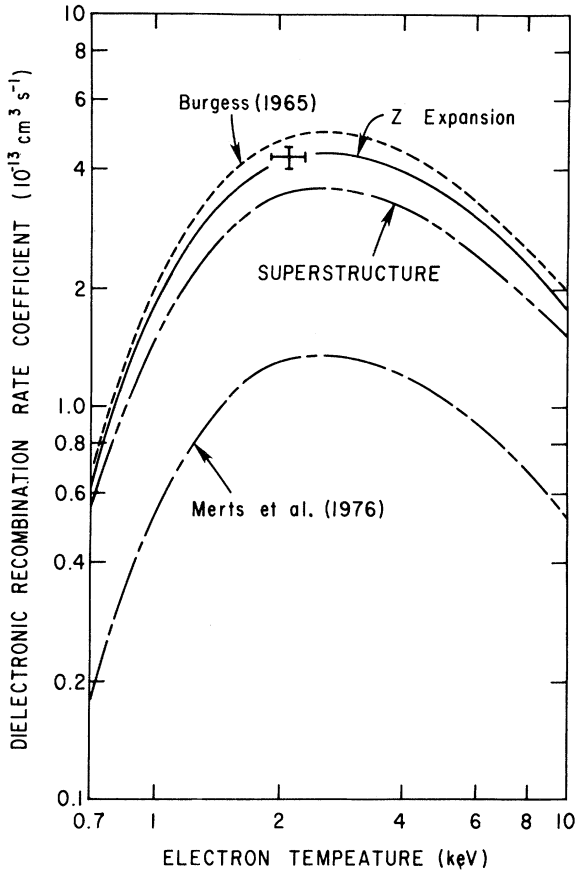

FIG. 10. Experimental value and theoretical predictions for the dielectronic recombination rate coefficient α_d of Ti XXII from the Z-expansion method, SUPERSTRUCTURE, Burgess (Ref. 44), and Merts *et al.* (Ref. 45). The error bars mainly result from the experimental error of the laser Thomson scattering data.

bution was of the order of the experimental error for α_d. The error bars shown in Fig. 10 mainly result from the experimental error of the laser Thomson scattering data which were used for determination of the electron temperature.

Also shown in Fig. 10 are the predictions for the dielectronic recombination rate coefficient of Ti XXII from the present detailed calculations and from the formulas of Burgess[44] and Merts *et al.*[45] The experimental value for α_d is in agreement with the prediction from the Z-expansion method and it is only slightly larger than the theoretical value obtained from the SUPERSTRUCTURE calculations. [The differences in the predictions from the Z-expansion method and the SUPERSTRUCTURE calculations are due to the slightly different values obtained for the line factors $F_2(s)$.] Since the experimental point is at the maximum of the theoretical curve, this small difference is not masked by the error of the electron-temperature measurement.

VI. CONCLUSION

Dielectronic-satellite spectra of hydrogenlike titanium Ti XXII have been observed from PLT tokamak plasmas and have been used for a detailed comparison with the theoretical results obtained from the Z-expansion method and from SUPERSTRUCTURE. The results from the Z-expansion method are in excellent agreement with the experimental data except for minor discrepancies between theoretical and experimental wavelengths of 0.0003 Å for the $n=2$ satellites and 0.0001 Å for the separation of the Ly-α_1 and Ly-α_2 lines. The latter discrepancy is removed if the Lamb shift and relativistic effects of order α^4 are taken into account. Very good agreement with the experimental data is also obtained for the results from SUPERSTRUCTURE, although the discrepancies between the theoretical and experimental wavelengths $\simeq$0.0009 Å for the $n=2$ satellites are slightly larger.

The experimental data have also been used to determine the central ion and electron temperature of PLT discharges and to measure the dielectronic recombination rate coefficient α_d of Ti XXII. The experimental value for α_d is in good general agreement with the predictions from both the detailed calculations and Burgess's general formula.[44]

ACKNOWLEDGMENTS

The support of Dr. H. P. Furth, Dr. D. M. Meade, Dr. P. H. Rutherford, and Dr. J. C. Hosea is gratefully acknowledged. We appreciate the discussions with Dr. J. P. Briand, Dr. M. Marrus, Dr. E. Hinnov, and Dr. S. Suckewer. We also gratefully acknowledge the technical assistance of S. Winje, J. Gorman, J. Lehner, W. Urstadt, and the PLT technician crew under W. Mycock and assistance of the data processing group under R. Lusen. This work was supported by U.S. Department of Energy Contract No. DE-AC02-76-CHO-3073.

[1]G. W. Erickson, J. Phys. Chem. Ref. Data 6, 831 (1977).
[2]Y. I. Grineva, V. I. Karov, V. V. Korneev, V. V. Krutov, S. L. Mandelstam, L. A. Vainshtein, B. N. Vasilysev, and J. A. Zhitnik, Sol. Phys. 29, 441 (1973).
[3]A. H. Gabriel, J. L. Culhane, L. W. Acton, E. Antonucci, R. D. Bentley, C. Jordan, L. W. Leibacher, A. N. Parmar, K. J. H. Phillips, C. G. Rapley, C. J. Wolfson, and K. T. Strong, Adv. Space Res. 1, 267 (1981).
[4]M. Bitter, K. W. Hill, N. R. Sauthoff, P. C. Efthimion, E. Meservey, W. Roney, S. von Goeler, R. Horton, M. Goldman, and W. Stodiek, Phys. Rev. Lett. 43, 129 (1979).
[5]M. Bitter, S. von Goeler, K. W. Hill, R. Horton, D. Johnson, W. Roney, N. Sauthoff, E. Silver, and W. Stodiek, Phys. Rev. Lett. 47, 921 (1981).
[6]T. F. R. Group, J. Dubau, and M. Loulergue, J. Phys. B 15, 1007 (1982).

[7]F. Bely-Dubau, P. Faucher, L. Steenman-Clark, M. Bitter, S. von Goeler, K. W. Hill, C. Camhy-Val, and J. Dubau, Phys. Rev. A 26, 3459 (1982).
[8]R. Marrus, in *Beam-Foil Spectroscopy,* edited by S. Bashkin (Springer, New York, 1976), Vol. I, p. 209.
[9]J. P. Briand, M. Tavernier, P. Indelicato, R. Marrus, and H. Gould, Phys. Rev. Lett. 50, 932 (1983).
[10]V. A. Boiko, A. Ya. Faenov, S. A. Pikuz, and U. I. Safronova, Mon. Not. R. Astron. Soc. 181, 107 (1977).
[11]P. Indelicato, J. P. Briand, M. Tavernier, R. Marrus, and H. Gould, Bull. Am. Soc. 28, 926 (1983).
[12]C. Breton, C. De Michelis, M. Finkenthal, and M. Mattioli, Fontenay-aux-Roses Laboratory Report No. EUR-CEA-FC-948, 1978 (unpublished).
[13]K. Brau, S. von Goeler, M. Bitter, R. D. Cowan, D. Eames, K. Hill, N. Sauthoff, E. Silver, and W. Stodiek, Phys. Rev. A 22, 2769 (1980).
[14]M. Bitter, S. von Goeler, N. Sauthoff, K. W. Hill, K. Brau, D. Eames, M. Goldman, E. Silver, and W. Stodiek, in *Inner-Shell and X-Ray Physics of Atomics and Solids* (Plenum, New York, 1981), p. 861.
[15]W. Stodiek *et al.*, in *Plasmas Physics and Controlled Nuclear Fusion Research 1980,* Proceedings of the Eighth International Conference on Plasma Physics and Nuclear Fusion Research, Brussels, 1980 (IAEA, Vienna, 1981), Vol. I, p. 9 (unpublished).
[16]S. M. Younger, Phys. Rev. A 22, 111 (1980).
[17]D. Manos, D. Ruzic, R. Moore, and S. Cohen, J. Vac. Sci. Technol. 20, 1230 (1982).
[18]R. A. Boie, J. Fischer, Y. Inagaki, F. C. Merritt, V. Radeka, L. C. Rogers, and D. M. Xi, Nucl. Instrum. Methods 201, 93 (1982).
[19]H. Johann, Z. Phys. 69, 189 (1931)
[20]R. Hawryluk *et al.*, Phys. Rev. Lett. 49, 326 (1982).
[21]M. Bitter, S. von Goeler, M. Goldman, K. W. Hill, R. Horton, W. Roney, N. Sauthoff, and W. Stodiek, in *Temperature, Its Measurement and Control in Science and Industry,* edited by J. F. Schooley (American Institute of Physics, New York, 1982), Vol. 5, p. 693.
[22]S. von Goeler, M. Bitter, S. Cohen, D. Eames, K. W. Hill, D. Hills, R. Hulse, G. Lenner, D. Manos, P. Roney, W. Roney, N. Sauthoff, S. Sesnic, W. Stodiek, F. Tenney, and J. Timberlake, in *Proceedings of the Course on Diagnostics for Fusion Reactor Conditions, Varenna, Italy, 1982,* edited by P. E. Stott *et al.* (Commission of the European Communities, Brussels, 1983), Vol. I, p. 109.
[23]E. Källne, J. Källne, and J. E. Rice, Phys. Rev. Lett. 49, 330 (1982).
[24]G. A. Doschek, R. W. Kreplin, and U. Feldman, Astrophys. J. 233, L157 (1979).
[25]A. N. Parmar, J. L. Culhane, C. G. Rapley, E. Antonucci, and A. H. Gabriel, Mon. Not. R. Astron. Soc. 197, 29 (1981).
[26]F. Moriyami, K. Tanaka, K. Akita, T. Watanabe, H. Miyazaki, M. Miyashita, K. Kumagai, and K. Nishi, Annals of the Tokyo Astronomical Observatory, 2nd Series, Vol. XIX, No. 2 (1983).
[27]I. L. Beigman, L. A. Bureeva, and I. Yu. Skobolev, Astron. Zh. 56(6), 1281 (1979) [Sov. Astron. 23(6), 725 (1979)].
[28]U. I. Safronova, J. Quant. Spectrosc. Radiat. Transfer 15, 231 (1975).
[29]J. Dubau, A. H. Gabriel, M. Loulergue, L. Steenman-Clark, and S. Volonte, Mon. Not. R. Astron. Soc. 195, 705 (1981).
[30]J. Dubau, M. Loulergue, and L. Steenman-Clark, Mon. Not. R. Astron. Soc. 190, 125 (1980).
[31]U. I. Safronova, A. M. Urnov, and L. A. Vainshtein, Proc. P.N. Lebedev, Phys. Inst. [Acad. Sci. USSR 119, 13 (1980)].
[32]U. I. Safronova and A. F. Shestakov, Institute of Spectroscopy Report No. 7, Troitzk, 1976 (unpublished).
[33]B. W. Shore, Astrophys. J. 158, 1205 (1969).
[34]F. Bely-Dubau, A. H. Gabriel, and S. Volonte, Mon. Not. R. Astron. Soc. 189, 801 (1979).
[35]H. A. Bethe and E. E. Salpeter, *Quantum Mechanics of One- and Two-Electron Atoms* (Springer, Berlin, 1957).
[36]G. Breit and E. Teller, Astrophys. J. 91, 215 (1940).
[37]G. F. W. Drake, Phys. Rev. A 3, 908 (1971).
[38]A. H. Gabriel and T. M. Paget, J. Phys. B 5, 673 (1972).
[39]P. Faucher and S. Volonte (private communication).
[40]F. Bely-Dubau, J. Dubau, P. Faucher, and A. H. Gabriel, Mon. Not. R. Astron. Soc. 198, 239 (1982).
[41]I. I. Sobelman, L. A. Vainshtein, and E. A. Yukov, *Excitation of Atoms and Broadening of Spectral Lines,* Vol. 7 of *Chemical Physics,* edited by J. P. Toennies (Springer, New York, 1980).
[42]B. N. Chichkov, M. A. Mazing, A. P. Shevelko, and A. M. Urnov, Phys. Lett. 83A, 401 (1981).
[43]F. Bely-Dubau, M. Bitter, J. Dubau, P. Faucher, A. H. Gabriel, K. W. Hill, S. von Goeler, N. Sauthoff, and S. Volonte, Phys. Lett. 93A, 189 (1983).
[44]A. Burgess, Astrophys. J. 141, 1588 (1965).
[45]A. L. Merts, R. D. Cowan, and N. H. Magree, Los Alamos Scientific Laboratory Report No. LA-6220-MS, 1976 (unpublished).